

Diffuse axonal injury in mild traumatic brain injury: a 3D multivoxel proton MR spectroscopy study

Ivan I. Kirov · Assaf Tal · James S. Babb ·
Yvonne W. Lui · Robert I. Grossman ·
Oded Gonen

Received: 13 April 2012 / Revised: 12 June 2012 / Accepted: 14 July 2012
© Springer-Verlag 2012

Abstract Since mild traumatic brain injury (mTBI) often leads to neurological symptoms even without clinical MRI findings, our goal was to test whether diffuse axonal injury is quantifiable with multivoxel proton MR spectroscopic imaging ($^1\text{H-MRSI}$). T1- and T2-weighted MRI images and three-dimensional $^1\text{H-MRSI}$ (480 voxels over 360 cm^3 , about 30 % of the brain) were acquired at 3 T from 26 mTBI patients (mean Glasgow Coma Scale score 14.7, 18–56 years old, 3–55 days after injury) and 13 healthy matched contemporaries as controls. The *N*-acetylaspartate (NAA), choline (Cho), creatine (Cr) and *myo*-inositol (*mI*) concentrations and gray-matter/white-matter (GM/WM) and cerebrospinal fluid fractions were obtained in each voxel. Global GM and WM absolute metabolic concentrations were estimated using linear regression, and patients were compared with controls using two-way analysis of variance. In patients, mean NAA, Cr, Cho and *mI* concentrations in GM (8.4 ± 0.7 , 6.9 ± 0.6 , 1.3 ± 0.2 , $5.5 \pm 0.6\text{ mM}$) and Cr, Cho and *mI* in WM (4.8 ± 0.5 , 1.4 ± 0.2 , $4.6 \pm 0.7\text{ mM}$) were not different from the values in controls. The NAA concentrations in WM, however, were significantly lower in patients than in controls (7.2 ± 0.8 vs. $7.7 \pm 0.6\text{ mM}$, $p = 0.0125$). The Cho and Cr levels in WM of patients were positively correlated with time since mTBI. This $^1\text{H-MRSI}$ approach allowed us to ascertain that early mTBI sequelae are (1) diffuse (not merely local), (2) neuronal (not glial), and (3) in the global WM (not GM). These findings support the hypothesis that,

similar to more severe head trauma, mTBI also results in diffuse axonal injury, but that dysfunction rather than cell death dominates shortly after injury.

Keywords Brain injury · Diffuse axonal injury · Magnetic resonance spectroscopy

Introduction

Traumatic brain injury (TBI) annually accounts for 1.6 million emergency room visits and hospitalizations in the US [1]. It is suspected that many more victims do not seek medical attention or are seen at their doctor's office. Patients who do not recover add to the 1 % of the US population living with TBI-related, long-term disability [2]. Moreover, TBI from blast exposure has been described as the "signature injury" of the recent wars in Iraq and Afghanistan [3] with about 20 % of veterans reporting probable mild TBI (mTBI) [4].

Characterized by less than a 30 min loss of consciousness (LOC), posttraumatic amnesia under 24 h and a Glasgow Coma Scale (GCS) score of 15–13 [5], mTBI is the most common (about 85 %) head trauma in both the military and civilian setting [6]. While most patients experience full symptom resolution within months, from 5 % to 15 % are diagnosed with persistent postconcussive syndrome to become what has been labeled the "miserable minority" [7].

TBI damage is assumed to result from the mechanical strain of sudden acceleration and deceleration that damages the axonal cytoskeleton and disrupts ionic balances. Abnormally high calcium influx impairs transport along the axon and can lead to dysfunction or axotomy followed by cell death [8, 9]. This strain can also cause vascular damage, seen by clinical MRI and CT and crucial for the acute

I. I. Kirov · A. Tal · J. S. Babb · Y. W. Lui ·
R. I. Grossman · O. Gonen (✉)
Department of Radiology, New York University School
of Medicine, 660 First Avenue, 4th Floor,
New York, NY 10016, USA
e-mail: oded.gonen@med.nyu.edu

assessment of mTBI: hemorrhages, hemosiderin and enlarged Virchow-Robin spaces [10]. All of these are presumed to be associated with underlying diffuse axonal injury (DAI) [11] which, however, is usually MRI and CT occult. This inability to assess the total disease load leads to weak correlation of imaging with clinical metrics [12], and motivates the search for other mTBI biomarkers to direct pharmacological regimens and predict outcome.

MRI-occult mTBI damage can be studied with quantitative MR methods, e.g., diffusion tensor [13], functional MRI [14], and proton MR spectroscopy ($^1\text{H-MRS}$) [15]. $^1\text{H-MRS}$ adds unique specificity to pathological processes by quantifying surrogates: *N*-acetylaspartate (NAA) for neuronal integrity, creatine (Cr) for cellular energy/density, choline (Cho) for membrane turnover and *myo*-inositol (*mI*) for astroglial proliferation [15]. Most studies, however, have used single-voxel or 2D $^1\text{H-MRS}$ covering under 10 % of the brain, regions-of-interest (ROIs) that may not be globally representative and that also make it impossible to distinguish focal from diffuse injury. In addition, quantification with metabolite ratios may confound interpretation since Cr (a frequent denominator) levels can also be abnormal [16, 17].

These shortcomings can be reduced with absolute metabolic quantification in multivoxel $^1\text{H-MRS}$ imaging ($^1\text{H-MRSI}$) over a much larger brain volume [18, 19]. Analyzing all voxels together improves the signal-to-noise ratio (SNR) for better precision, i.e., sensitivity to smaller global changes [20], at the cost of averaging out regional metabolic variations, a reasonable trade-off for diffuse disorders. Since mTBI often leads to neurological symptoms even without clinical MRI findings, our goal was to test if DAI is quantifiable by $^1\text{H-MRSI}$.

Materials and methods

Subjects

Twenty-six patients with closed-head mTBI (5 women, 21 men), aged 33 ± 11 years (mean \pm standard deviation; range 18–56 years), were recruited serially. Twenty-five were enrolled following emergency room visits with GCS score of 15–13 and confirmed LOC of 30 min or less. Patient 13 was referred from a physician's office, where mTBI diagnosis was based on clinical evaluation and 30 min LOC. Exclusion criteria were any MRI contraindications, substance dependencies, inability to give informed consent, HIV infection, prior TBI and history of any neurological disease. Patient demographics are presented in Table 1. Thirteen age- and gender-matched healthy controls (5 women, 8 men), aged 33 ± 12 years (range 19–57 years) were enrolled. Their exclusion criteria were the same as for

the patients, plus any findings on their T1- and T2-weighted MRI. The study was approved by the institutional ethics committee and was in accordance with the ethical standards of the 1964 Declaration of Helsinki and all participants gave written informed consent.

MR data acquisition

All experiments were done in a 3-T MRI scanner (Trio; Siemens AG, Erlangen, Germany) with a TEM3000 (MR Instruments, Minneapolis, MN) circularly polarized transmit–receive head coil. For image guidance of the $^1\text{H-MRSI}$ volume-of-interest (VOI), we acquired 30 3.7-mm thick axial T2-weighted fluid-attenuated inversion recovery (FLAIR) images: TE/TI/TR 88/2,500/9,000 ms, 256×256 mm field-of-view (FOV) and 512×512 matrix. For tissue segmentation, we acquired sagittal magnetization prepared rapid gradient echo (MP-RAGE): TE/TI/TR 2.6/800/1,360 ms, $256 \times 256 \times 160$ mm FOV and $256 \times 256 \times 160$ matrix. The MP-RAGE was reconstructed in axial, sagittal and coronal slices (1 mm^3 isotropic pixels) at an angle rendering the genu and splenium of the corpus callosum in the same horizontal plane at the level of the longitudinal fissure, as shown in Fig. 1a.

Our auto-shim procedure based on chemical shift imaging (CSI) then adjusted the scanner's first- and second-order currents in 3–5 min [21]. Next, a 360-cm^3 $^1\text{H-MRSI}$ VOI ($10 \times 8 \times 4.5$ cm, anterior–posterior \times left–right \times inferior–superior, AP \times LR \times IS) was image-guided over the corpus callosum, as shown in Fig. 1. The VOI was excited with TE/TR 35/1,800 ms PRESS in three 1.5-cm thick, second-order Hadamard encoded slabs (six slices) interleaved every TR in the IS direction (Fig. 1c) for optimal SNR and spatial coverage [22]. These slices were partitioned with 2D 16×16 CSI over a 16×16 -cm FOV to yield $1.0 \times 1.0 \times 0.75$ -cm nominal voxels as shown in Fig. 1. The 8×10 -cm (LR \times AP) VOI was defined in their planes with two 11.2-ms long numerically optimized 180° RF pulses (4.5 kHz bandwidth) under 1.34 and 1.1 mT/m gradients to yield $8 \times 10 \times 6 = 480$ voxels. The MR signal was acquired for 256 ms at ± 1 kHz bandwidth. At two averages, the $^1\text{H-MRSI}$ took 34 min and the entire protocol less than an hour.

Voxel tissue segmentation

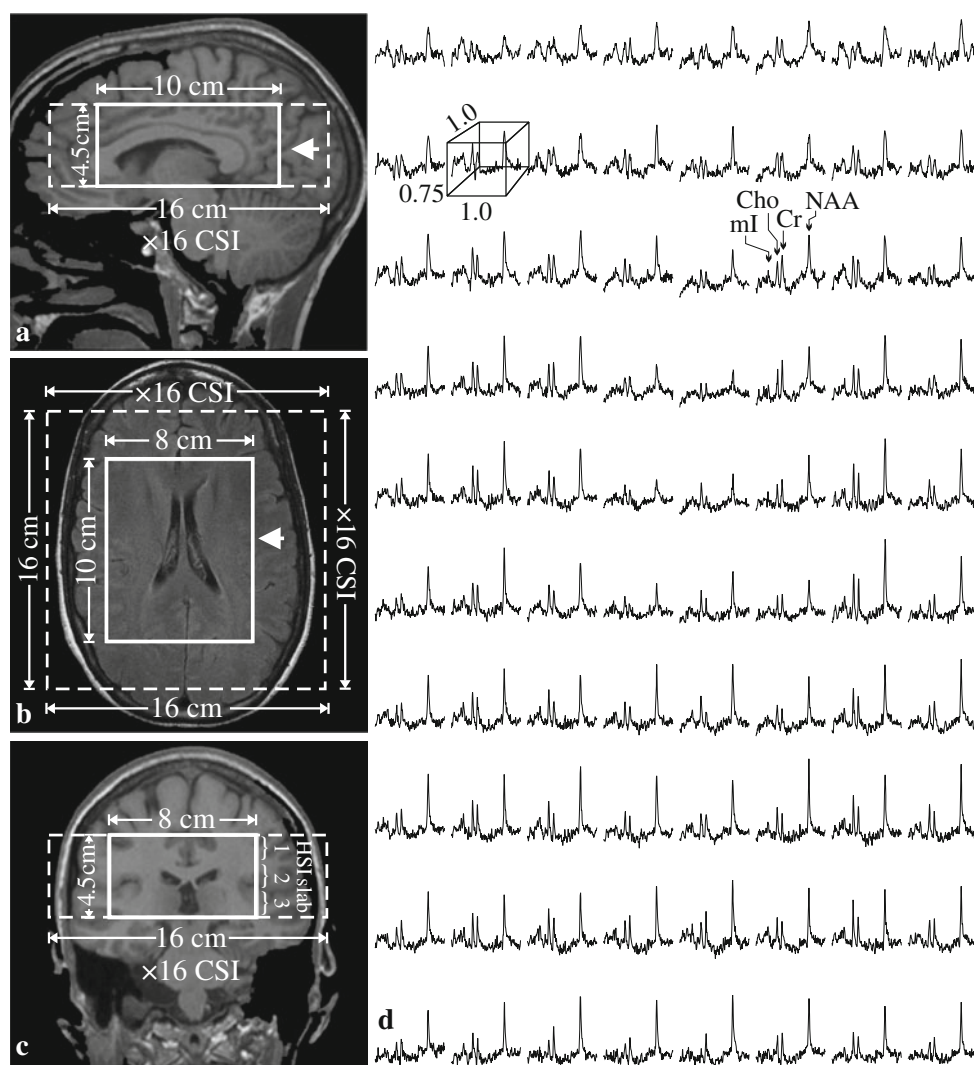
The MP-RAGE images were segmented using SPM2 (Wellcome Department of Cognitive Neurology, Institute of Neurology, London, UK [23]) to obtain CSF, WM and GM masks. These were coregistered with the $^1\text{H-MRSI}$ grid using in-house software (MATLAB 2009b; The MathWorks Inc., Natick, MA), as shown in Fig. 2, yielding their volume contribution to every *j*th voxel in the *k*th subject: V_{jk}^{GM} , V_{jk}^{WM} , V_{jk}^{CSF} .

Table 1 Patient demographics and imaging findings (with the patients sorted by time since mTBI)

Patient	Age	Gender	TBI cause	GCS score	LOC duration (min)	Time since injury (days)	Self-reported symptoms on scan date ^a	MRI findings
1	40	M	Fall	15	3	3	NS, V	Unremarkable
2	41	M	Fall	15	<1	5	NS, H, D, S	Unremarkable
3	42	M	Fall	14	5	5	H, N, S, M	Unremarkable
4	22	M	Assault	13	30	6	NS, H, N, P	Unremarkable
5	18	M	Assault	15	20	10	None	Unremarkable
6	25	M	Assault	15	25	10	H	Right frontal convexity arachnoid cyst
7	27	M	Assault	15	<1	12	None	Unremarkable
8	29	M	Bike fall	15	15	13	None	Unremarkable
9	25	F	Pedestrian struck by car	15	2	14	None	Unremarkable
10	32	M	Assault	15	2	17	H, D, S, M	Unremarkable
11	23	M	Assault	14	30	18	None	Two ovoid foci of abnormal T2 hyperintensities in left frontal lobe subcortical white matter with nonspecific etiology
12	23	M	Assault	15	30	18	NS, H, D, N, M	Unremarkable
13	24	M	Assault	n/a	30	18	None	Unremarkable
14	18	M	Pedestrian struck by car	15	15	19	H, D, M	Unremarkable
15	19	M	Assault	14	30	19	None	Unremarkable
16	51	M	Motor vehicle accident	14	30	19	NS, H	Few punctate foci of abnormal T2 hyperintensities in frontal and parietal lobe subcortical white matter with nonspecific etiology
17	37	M	Fall	15	2	20	NS, H, D, N, P	Unremarkable
18	51	F	Bike fall	14	30	20	NS, H, D, N, P, S, PH	Stable right cerebellopontine angle arachnoid cyst
19	36	M	Fall	15	<1	23	None	Unremarkable
20	35	M	Sport collision	15	<1	24	None	Unremarkable
21	28	F	Cyclist struck by car	15	20	29	NS, H, D, N, P, S	Unremarkable
22	38	M	Fall	15	<1	31	None	Unremarkable
23	56	M	Assault	15	<1	40	NS, P	Unremarkable
24	32	F	Fall	15	1	43	NS, D, M	Unremarkable
25	44	F	Pedestrian struck by car	15	<1	54	D, P, M	Unremarkable
26	50	M	Fall	15	<1	55	NS, H, D, N, P, S, M, PH	Unremarkable
Average ± standard deviation	33 ± 11			14.7 ± 0.5	12 ± 13	21 ± 14		

^a Most to least common: *H* headache, *NS* neck stiffness, *D* dizziness, *M* memory deficits, *N* nausea, *P* photophobia, *S* sleep disturbance, *PH* paresthesia (hand), *V* blurred vision.

Fig. 1 *Left* Positioning of the ^1H -MRS VOI: sagittal T1-weighted (a), axial T2-weighted (b), and coronal T1-weighted (c) MR images in patient 18, with the VOI ($8 \times 10 \times 4.5$ cm, LR \times AP \times IS; *thick solid white lines*) and FOV ($16 \times 16 \times 4.5$ cm; *dashed white lines*) superimposed; the *arrow* on each image indicates the spatial position of the image below. *Right* (d) Real part of the 8×10 (LR \times AP) ^1H spectra matrix from the VOI on the axial image. All spectra are on common frequency (1.3–3.9 ppm) and intensity scales. Note the SNR and spectral resolution obtained from these $1.0 \times 1.0 \times 0.75$ -cm (LR \times AP \times IS) voxels in an acquisition time of about 30 min



Metabolic quantification

The ^1H -MRSI data were processed offline using in-house software written in IDL (Research Systems Inc., Boulder, CO). The data were voxel-shifted to align the NAA grid with the VOI. The data were then Fourier-transformed in the time, AP and LR dimensions and Hadamard-reconstructed along the IS direction. The 480 spectra were each frequency-aligned and zero-order phase-corrected in reference to the NAA peak. Voxels which demonstrated lipid contamination were excluded from the analysis.

Relative levels of the i th ($i = \text{NAA}, \text{Cr}, \text{Cho}, \text{mI}$) metabolite in the j th ($j = 1, \dots, 480$) voxel in the k th ($k = 1, \dots, 39$) subject were obtained from their peak area, S_{ijk} , using SITools-FITT parametric spectral modeling software package [24]. The S_{ijk} -s were scaled into absolute millimole amounts, Q_{ijk} , relative to a 2-L sphere of $C_i^{\text{vitro}} = 12.5, 10.0, 3.0$ and 7.5 mM NAA, Cr, Cho and mI in water:

$$Q_{ijk} = \frac{C_i^{\text{vitro}}}{V} \cdot \frac{S_{ijk}}{S_{ijR}} \cdot \left(\frac{P_j^{180^\circ}}{P_R^{180^\circ}} \right)^{\frac{1}{2}} \text{ mmol}, \quad (1)$$

where V is the voxel volume, S_{ijR} is the metabolite signal from the voxels of the sphere, $P_j^{180^\circ}$ and $P_R^{180^\circ}$ the RF power for a nonselective 1 ms 180° inversion pulse on the k th subject and reference.

Average VOI tissue concentrations, Q_{ik} , were corrected for the relaxation time differences between each metabolite, i , in vivo ($T_1^{\text{vivo}}, T_2^{\text{vivo}}$) and in the phantom ($T_1^{\text{vitro}}, T_2^{\text{vitro}}$) with:

$$f_i = \frac{\exp(-TE/T_2^{\text{vitro}})}{\exp(-TE/T_2^{\text{vivo}})} \cdot \frac{1 - \exp(-TR/T_2^{\text{vitro}})}{1 - \exp(-TR/T_2^{\text{vivo}})}. \quad (2)$$

Literature 3-T T_1^{vivo} [25] and T_2^{vivo} values [26, 27] were used. If values for GM and WM were reported separately, a weighted average of 3:2 WM:GM (the composition of the VOI) was calculated. For NAA, Cr, Cho and mI the T_1^{vivo}

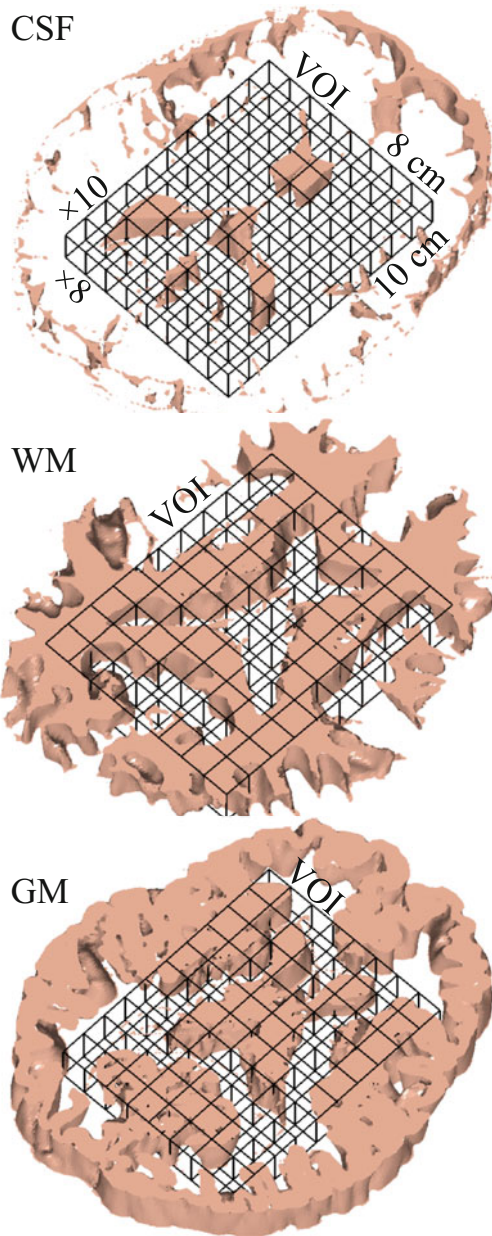


Fig. 2 ¹H-MRS MRI coregistration. 3D renderings of one of the six 7.5-mm thick spectroscopic slices in patient 12 in Table 1, coregistered with its 7.5 corresponding CSF, WM and GM masks (1 mm thick each) segmented from the T1-weighted MR images using SPM. Our in-house software counted how many pixels of each mask fell into every spectroscopic voxel in the VOI to estimate its volume for the analysis of Eqs. 3 and 4

values were 1,360, 1,300, 1,145 and 1,170 ms and the T_2^{vivo} values were 350, 174, 251 and 200 ms. The corresponding values measured in the phantom were T_2^{vitro} 483, 288, 200 and 233 ms, and T_1^{vitro} 605, 336, 235 and 280 ms.

The average tissue concentration in the VOI for each metabolite, C_{ik} was obtained as:

$$C_{ik} = \frac{\sum_{j=1}^{480} Q_{ijk}}{\sum_{j=1}^{480} (V_{jk}^{\text{GM}} + V_{jk}^{\text{WM}})} \cdot f_i \text{ mM/g wet weight} \quad (3)$$

The sum of all voxels, C_{ik} , has the advantage of about a 22-fold lower variance [(number of voxels)^{1/2}] than individual voxels, and consequently is expected to yield better precision [20].

Global WM and GM concentrations

Since the CSF does not contribute to the ¹H-MRSI signals, the *i*th metabolite amount in the *j*th voxel in the *k*th subject can be modeled as a sum of two compartments (GM, WM):

$$\begin{aligned} Q_{ijk} &= Q_{ijk}^{\text{GM}} + Q_{ijk}^{\text{WM}} \\ &= C_{ik}^{\text{GM}} \cdot V_{jk}^{\text{GM}} \cdot f_i^{\text{GM}} + C_{ik}^{\text{WM}} \cdot V_{jk}^{\text{WM}} \cdot f_i^{\text{WM}}, \end{aligned} \quad (4)$$

where C_{ik}^{WM} and C_{ik}^{GM} are the *k*th subject *i*th metabolite (unknown) global WM and GM concentrations and f_i^{GM} , f_i^{WM} are given by Eq. 2 with T_2^{vivo} values of 275, 157, 241 and 200 ms for NAA, Cr, Cho and *mI* in GM, and 400, 185, 258 and 200 ms in WM [26, 27]. The GM and WM T_1^{vivo} , T_2^{vitro} s and T_1^{vitro} s are the same as in Eq. 2 above.

Although C_{ik}^{WM} and C_{ik}^{GM} cannot both be derived from Eq. 4, since the brain's GM and WM heterogeneity is on a scale smaller than the 1 cm³ ¹H-MRSI voxels, each voxel will have different V_{jk}^{WM} and V_{jk}^{GM} independent coefficients. The resulting over-determined 480 equation system was therefore solved for the optimal C_{ik}^{WM} and C_{ik}^{GM} using linear regression [19].

Statistical analyses

Two-way analysis of variance was used to compare the means of each metabolite between patients and controls. A separate analysis was conducted for each metabolite globally, and in WM and GM. In each case, the observed metabolite values constituted the dependent variable, while the model included subject group as a classification factor and the error variance was allowed to differ across subject groups to remove the unnecessary assumption of variance homogeneity. Since controls were matched to patients in age and gender, the indicator variable identifying subjects that were matched was included in the model as a blocking factor. As a result, the comparisons of global and tissue-specific concentrations were adjusted for age and gender. Reported *p* values are two-sided, defined as significant for *p* < 0.05, except for NAA. Since it is known to always be lower in all adult neuropathologies we looked for single-sided *p* values. Pearson and Spearman correlations were used to look for relationships between concentrations and

time since injury. SAS 9.0 (SAS Institute, Cary, NC) was used for all computations.

Results

In the patients the GCS score was 14.7 ± 0.5 (mean \pm standard deviation) and the mean time since injury was 21 days (range 3–55 days), as shown in Table 1. Of the four mTBI patients who had positive MRI findings, in only two (patients 11 and 16) were the findings possibly directly related to their head trauma. Five patients were on medication for a trauma-induced symptom.

Our automatic shim yielded a consistent 26 ± 3 Hz whole-head FWHM water line that decreased to 21 ± 3 Hz in the VOI without additional adjustments. An example of a VOI (size, position and spectra) is shown in Fig. 1. Occasional lipid contamination caused up to at most ten voxels per dataset to be excluded from the analysis. The SNRs of the metabolites in the remaining approximately 18,720 voxels (39 subjects \times 480 voxels each) were NAA 30 ± 7 , Cr 15 ± 3 , Cho 13 ± 3 and *mI* 8 ± 1 , and the average linewidth was 6.6 ± 2.0 Hz. Under 1 % of the voxels contained >90 % GM and 20 % had WM fractions >90 %, i.e., could be considered “pure.”

The spectra summed from all the 480 VOI voxels (equivalent to the numerator of Eq. 3) from every subject overlaid with their fits are shown in Fig. 3. They exhibit NAA, Cr, Cho and *mI* SNRs of 561 ± 74 , 265 ± 34 , 228 ± 32 and 128 ± 17 , a dramatic 22-fold gain (approximately $480^{1/2}$) over the original 0.75-cm^3 voxels (compare Fig. 3 with Fig. 1d) and linewidths of 6.5 ± 0.6 Hz retaining the single-voxel spectral resolution [18].

The metabolic concentrations in patients and controls in the whole VOI (Eq. 3) as well as in its WM and GM moieties (Eq. 4) are given in Table 2, and their distributions are plotted in Fig. 4. Cr, Cho and *mI* concentrations in patients were not different from the concentrations in controls either in the VOI, or in the WM or GM. The NAA concentrations, however, were significantly lower in the VOI in patients (7.4 ± 0.6 vs. 7.9 ± 0.6 mM, $p = 0.0180$) and in their WM (7.2 ± 0.8 vs. 7.7 ± 0.6 mM, $p = 0.0125$) but not in the GM, as shown in Fig. 4. While the reduced VOI NAA concentrations showed a trend towards significance upon application of Bonferroni correction for multiple comparisons, the WM change remained significant. To take disease duration into account we looked for associations between all concentrations and time since injury, and found significant Pearson and Spearman correlations in WM Cho (0.004 mM/day, $r = 0.4$, $p = 0.043$, and $r = 0.43$, $p = 0.028$) and Pearson correlation in WM Cr (0.013 mM/day, $r = 0.39$, $p = 0.049$) as shown in Fig. 5.

Discussion

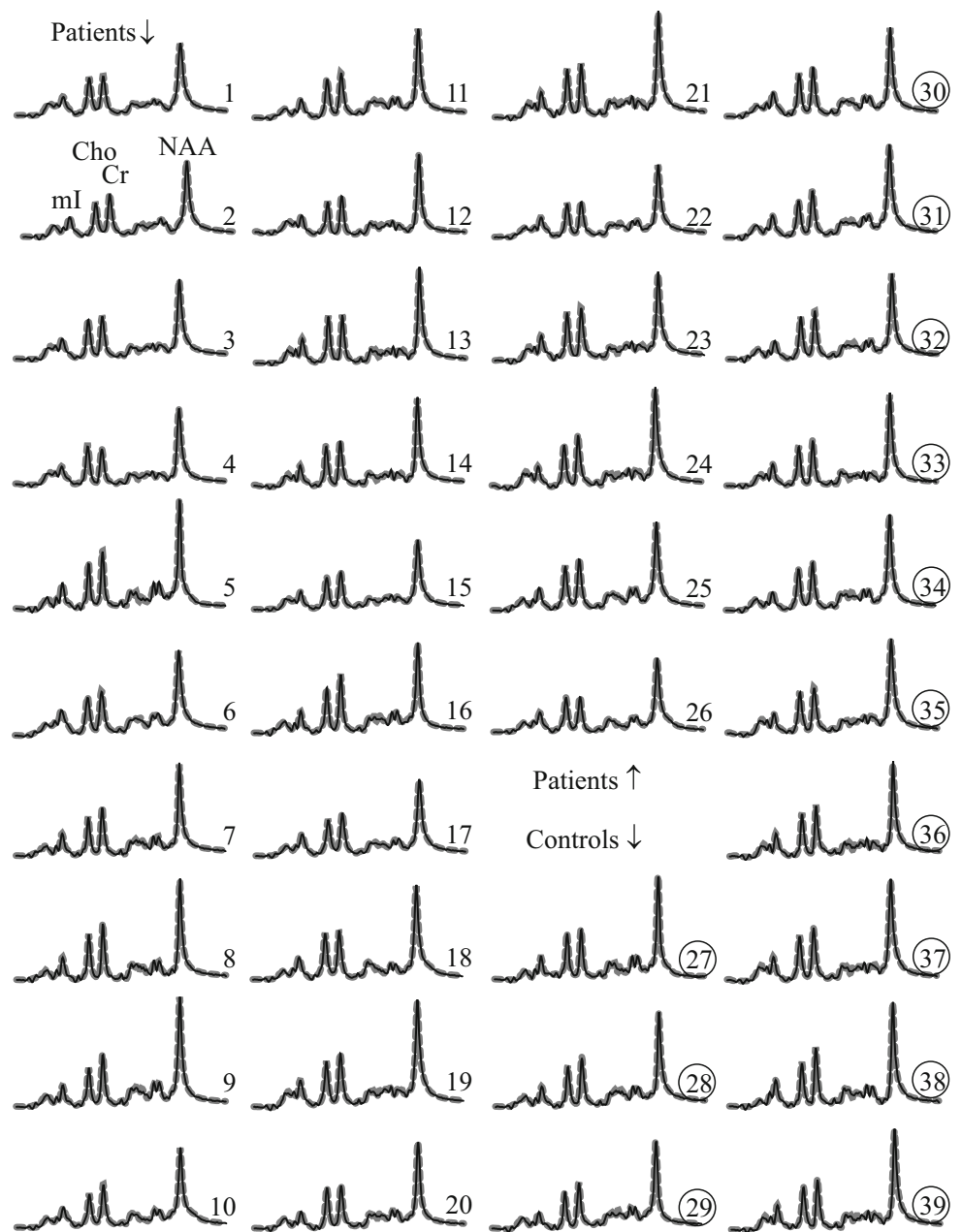
^1H -MRS sensitivity to mTBI

The advantages of ^1H -MRS over other quantitative MR techniques are specificity to injury type through the quantification of metabolites indicative of different processes, and sensitivity to nonstructural injury and to GM status. Since the first ^1H -MRS study of mTBI implicated the splenium of the corpus callosum [28], abnormalities have been reported in the parietal, temporal, occipital [29, 30] and frontal [30–33] lobes, pericontusional [34, 35] and supraventricular areas [16, 17]. However, in the same regions, some cohorts show abnormalities [17, 31] and others do not [29]. Direct comparisons of mTBI findings is difficult, however, due to different times since injury, injury heterogeneity, use of single-voxel ^1H -MRS and the use of metabolic ratios that assume stable Cr concentrations. For example, lower NAA/Cr ratios, which are usually attributed to NAA reductions, may be due to increased Cr [16, 17]. Indeed, following their pioneering study, Cecil et al. [28] attributed lower NAA/Cr in the splenium to a deficit in NAA, whereas absolute quantification in that structure revealed normal NAA and increased Cr [16]. Yet only four mTBI ^1H -MRS studies have used absolute quantification [16, 17, 30, 36], and just one in a substantial volume [30]. Although the latter also showed WM reduced NAA, it included patients with moderate TBI, and hence it is not directly comparable to our study.

Two main points can be deduced from past research. First, mTBI is likely a diffuse/multifocal condition with no specific region(s) consistently involved. Subjectively chosen ROIs, therefore, may miss pathology in some patients, reducing the statistical power and underscoring the need for extensive volume coverage. Second, higher sensitivity in ^1H -MRS is needed, e.g., of the 25 ROIs in one study, almost 70 % had consistent trends for abnormalities, without statistical significance [29]. With the use of single voxels, however, focal disease cannot be differentiated from diffuse disease, and SNR, spatial resolution (partial volume) and coverage must be balanced. Specifically, small ROIs may lack sensitivity and bigger ones suffer from a GM/WM/CSF partial volume effect that can lead to apparent variations in their metabolite levels, confounding the detection of injury-related changes (see the [cautionary note section](#) below).

To address both sensitivity and limited coverage and to test the hypothesis that mTBI results in diffuse sequelae, we used a large (360 cm^3) VOI in which every voxel's spectrum contributed to calculating the concentration of each metabolite [18, 19]. Analyzing many (480) voxels simultaneously increased the precision, reflected by a coefficient of variation in the controls of about 10 %, as

Fig. 3 Real part of the aligned and summed ^1H -MRS spectra from all the voxels in the VOI (thin black lines) representing Eq. 3 of each of the 26 patients (1–26) and 13 controls (27–39, circled). Each spectrum is shown with its fitted model function (thick dashed gray lines). All are on common intensity and chemical shift scales. Note the excellent SNRs and spectral resolution, as well as the visual similarity in Cr, Cho and mI levels between patients and controls versus decreased NAA



good or better than other ^1H -MRS methods. Importantly, any abnormalities detected this way must be diffuse since focal changes would be averaged out.

Diffuse abnormalities

It is well documented that TBI involves diffuse changes that may determine adverse outcomes [37, 38]. While hemorrhages are a marker for DAI on conventional imaging, most mTBI patients have unremarkable MRI/CT scans [11] and are rarely available for post-mortem study. Consequently, hypotheses on the pathology of mTBI are mostly based on histology of more severe TBI and animal models

that lack the heterogeneity of human injury [38]. Fortunately, indirect evidence of mTBI changes has been obtained by quantitative MR methods, e.g., DTI [13], functional MRI [14] and ^1H -MRS [15]. If the injury loci are different among patients [39], however, ROI-based studies cannot differentiate focal from diffuse injury. Our results support the DAI hypothesis in mTBI.

Axonal pathology

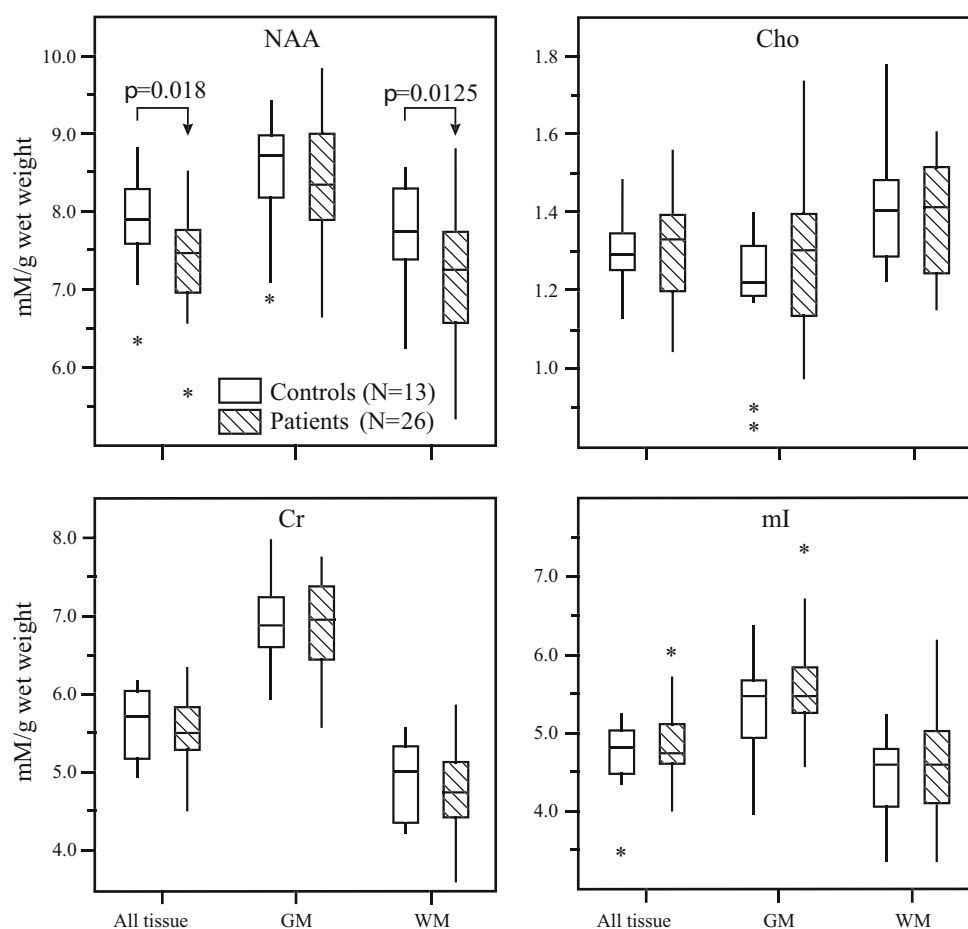
Axons are known to be vulnerable to the inertial forces of blunt head trauma. A large body of evidence from ex vivo animal and human TBI studies suggests that the initial site

Table 2 Metabolite concentrations (means \pm standard deviations) in the whole VOI (using Eq. 3) and in its WM and GM moieties (from Eq. 4) in each subject group

Tissue	Concentration (mM/g wet weight)			
	NAA	Cr	Cho	<i>mI</i>
Whole VOI				
Controls	7.9 \pm 0.6*	5.6 \pm 0.5	1.3 \pm 0.1	4.7 \pm 0.5
Patients	7.4 \pm 0.6*	5.5 \pm 0.5	1.3 \pm 0.1	4.8 \pm 0.5
WM				
Controls	7.7 \pm 0.6*	4.9 \pm 0.5	1.4 \pm 0.1	4.4 \pm 0.6
Patients	7.2 \pm 0.8*	4.8 \pm 0.5	1.4 \pm 0.2	4.6 \pm 0.7
GM				
Controls	8.5 \pm 0.7	6.9 \pm 0.6	1.2 \pm 0.2	5.3 \pm 0.6
Patients	8.4 \pm 0.7	6.9 \pm 0.6	1.3 \pm 0.2	5.5 \pm 0.6

* $p < 0.05$

Fig. 4 NAA, Cr, Cho and *mI* concentrations in the whole VOI (All tissue), GM and WM in mTBI patients and controls (boxes 25 %, median and 75 %; whiskers 95 %; asterisks outliers). The difference in NAA concentration in the whole VOI between patients and controls is significant, and the difference is entirely attributable to the pathology in the WM



of injury is the axolemma via disruption of ionic channels [38, 39]. Calcium influx impairs axonal transport, resulting in axonal swelling and potential axotomy [8, 9] that may be followed by Wallerian and retrograde degeneration and ultimately cell necrosis or apoptosis [9].

Cell death cannot be distinguished from dysfunction on the basis of the observed NAA decrease in the WM. The latter, however, is supported by the lack of difference in Cr, Cho and *mI* levels between patients and controls. Normal

Cho levels in patients may indicate absence of fragmented myelin from axon swelling or degeneration, as also suggested by DTI data [40]. Furthermore, normal *mI* and Cr levels that originate from intracellular stores in astrocytes [41] may represent lack of astroglial hypertrophy or hyperplasia from the astroglial scarring that typically forms on severed axons that is associated with permanent neuronal injury in more severe TBI [42]. In addition, normal NAA levels in the GM found in this and other mTBI

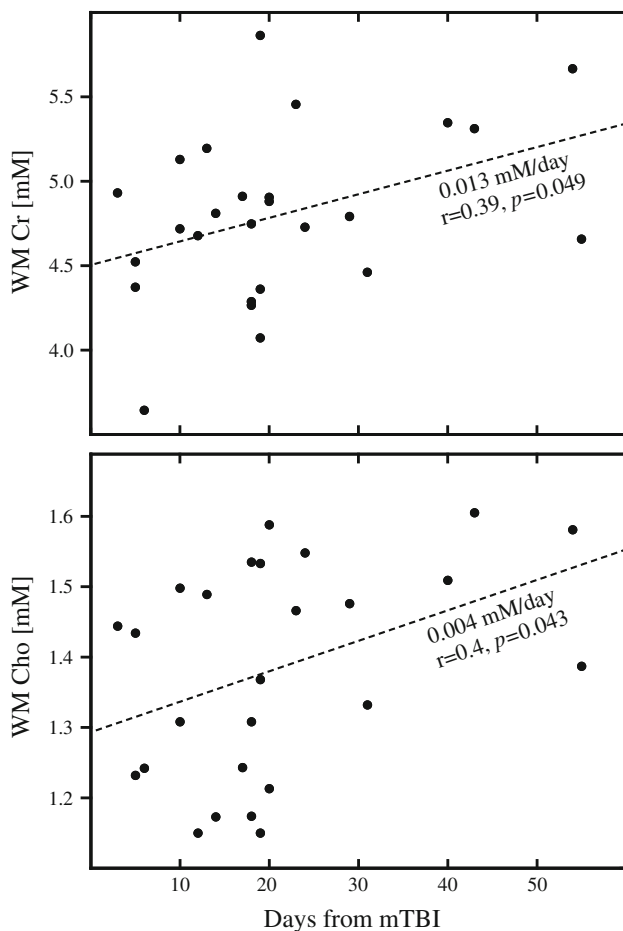


Fig. 5 Concentrations of Cr (*top*) and Cho (*bottom*) in the WM in relation to time since injury (in days) in each patient. The concentrations of both metabolites show a significant increase with time since injury. Such increases were not seen in the GM indicating possible evolving axonal pathology with sparing of the cell bodies

studies [16, 17] suggests no cell body injury from Wallerian degeneration. This process in humans, however, is thought to take several months [8], and it can be conjectured that the correlations between the increases in the concentrations of Cho and Cr with time in our cohort may represent progression. Given their cross-sectional nature, however, these correlations need to be interpreted with caution until verified in a longitudinal study.

While it is unclear whether cell death is characteristic of early mTBI, even if it occurs it is unlikely to be widespread [9, 39]. Rather, axons may convert to a dysfunctional state from which they may recover [9], as evidenced by NAA levels in serial ^1H -MRS studies [32, 33, 43]. Our data support the current consensus that brain injury is on a continuum [11, 39, 40], i.e., DAI occurs in mTBI to a lesser degree than in more severe trauma. In addition, if axonal dysfunction and not death dominates mTBI pathology, it is important to reiterate the danger of a second traumatic

event [39], and underscore potential benefits of suitable therapy.

Finally, only two patients (8 %) had (potentially) injury-related MRI findings, which would qualify their mTBI as “complicated” [11]. This is much lower than the 17 % rate of CT findings reported by Stein and Ross [44] in 1,538 patients, and may reflect the fact that 80 % of our patients had a GCS score of 15 that is associated with a 5 % findings rate [45]. Since it is well known that severity differs across the ‘mild’ range, i.e., not all GCS scores in mTBI are equivalent [46], it is noteworthy that our patient population suffered relatively milder (more subtle) injury than commonly seen in mTBI. Our results, therefore, suggest the presence of DAI in patients with mostly normal GCS scores and MRI scans, i.e., injury missed by the clinical and radiological examinations.

A cautionary note

Even at relatively high (0.75 cm^3) spatial resolution, only 20 % of the VOI voxels contained 90 % or more WM (considered “pure”) and under 1 % were over 90 % GM. The different GM and WM metabolite concentrations present a confounding scenario. Different placement (in a serial or cross-sectional study) could alter a voxel’s WM/GM fractions, and hence its ^1H -MRS signal, regardless of any underlying pathology. Since early changes in mTBI are small, placing a voxel in a WM region with an unaccounted for GM partial volume will boost its NAA signal (which is about 15 % higher in the GM) sufficiently to offset its pathology-associated deficit of about 7 % or cause enough change in the signal to render differences insignificant. This underscores the importance of tissue segmentation, and that attempts to place voxels in “pure” WM or GM to circumvent this confounding scenario are unlikely to be reliable.

Limitations

This study was also subject to some limitations. First, since it was geared to maximize sensitivity at the expense of localization (although the original 3D data remained available), it was insensitive to focal changes that may have occurred only in specific small brain region(s). For example, while Cr levels were normal in the global WM, this may not necessarily be the case locally [16, 17]. For our approach to yield significant differences, however, changes must be present in a substantial part of our VOI. Therefore this study demonstrated not the absence of local injury but rather the presence of a diffuse component. Second, while the study demonstrated that this diffuse injury is axonal, its correspondence to histopathologically defined DAI [8, 47] remains unclear. Also known as

“traumatic axonal injury”, DAI is characterized by the presence of axonal swellings which can only be conclusively diagnosed post mortem [47]. Structurally intact axons can also be affected [47], however, and diffusely lower NAA levels can represent manifestations of both types of DAI sequelae with an unknown contribution from each. Third is the assumption that GM and WM metabolite concentrations do not vary much over the VOI. While concentrations between tissue types differ significantly, within-tissue variations are small and in the forebrain exist only for NAA and Cho (mostly between the thalamus and cortical GM) [48]. If these differences were the same in all subjects, the only constraint would be that the changes be uniform (all increases or all decreases), a reasonable assumption given the decreases in NAA levels, and the increases in Cr, Cho and *mI* levels reported in TBI [15]. Fourth, although our VOI covered substantially more brain than most previous studies, it excluded most of the cortex (it contains about 40 %, of the approximate 470 cm³ WM volume of the brain [49], as well as cortical GM and all deep GM structures). Finally, the time required for acquisition and postprocessing may limit the clinical application of the technique in its current form.

Conclusion

We report evidence of DAI in patients with recent “non-complicated” mTBI assessed by global quantitative ¹H-MRS. The lack of glial WM abnormalities and any GM injury within 2 months of mTBI suggests white matter dysfunction rather than degeneration, and underscores the potential for axonal recovery.

Acknowledgments This work was supported by National Institutes of Health grants EB01015, NS39135, NS29029 and NS050520. Assaf Tal is also supported by the Human Frontiers Science Project. We thank Ms. Nissa Perry and Mr. Joseph Reaume for subject recruitment.

Conflicts of interest The authors declare that they have no conflict of interest.

Ethical standard This work has been approved by the appropriate ethics committee and therefore been performed in accordance with the ethical standards laid down in the 1964 Declaration of Helsinki.

References

- Faul M, Xu L, Wald M, Coronado V (2010) Traumatic brain injury in the United States: emergency department visits, hospitalizations and deaths, 2002–2006. Centers for Disease Control and Prevention, National Center for Injury Prevention and Control, Atlanta
- Zaloshnja E, Miller T, Langlois JA, Selassie AW (2008) Prevalence of long-term disability from traumatic brain injury in the civilian population of the United States, 2005. *J Head Trauma Rehabil* 23:394–400
- Snell FI, Halter MJ (2010) A signature wound of war: mild traumatic brain injury. *J Psychosoc Nurs Ment Health Serv* 48:22–28
- Tanelian T, Jaycox LH (2008) Invisible wounds of war report. RAND Corporation, Santa Monica, p 305
- Teasdale G, Jennett B (1974) Assessment of coma and impaired consciousness. A practical scale. *Lancet* 2:81–84
- MacGregor AJ, Shaffer RA, Dougherty AL, Galarneau MR, Raman R, Baker DG, Lindsay SP, Golomb BA, Corson KS (2010) Prevalence and psychological correlates of traumatic brain injury in operation Iraqi freedom. *J Head Trauma Rehabil* 25:1–8
- Ruff R (2005) Two decades of advances in understanding of mild traumatic brain injury. *J Head Trauma Rehabil* 20:5–18
- Buki A, Povlishock JT (2006) All roads lead to disconnection? – traumatic axonal injury revisited. *Acta Neurochir (Wien)* 148:181–193 (discussion 193–184)
- Iverson GL (2005) Outcome from mild traumatic brain injury. *Curr Opin Psychiatry* 18:301–317
- Inglese M, Bomszyk E, Gonen O, Mannon LJ, Grossman RI, Rusinek H (2005) Dilated perivascular spaces: hallmarks of mild traumatic brain injury. *AJNR Am J Neuroradiol* 26:719–724
- Bigler ED (2010) Neuroimaging in mild traumatic brain injury. *Psychol Injury Law* 3(1):36–49
- Wilson JT, Wiedmann KD, Hadley DM, Condon B, Teasdale G, Brooks DN (1988) Early and late magnetic resonance imaging and neuropsychological outcome after head injury. *J Neurol Neurosurg Psychiatry* 51:391–396
- Niogi SN, Mukherjee P (2010) Diffusion tensor imaging of mild traumatic brain injury. *J Head Trauma Rehabil* 25:241–255
- Mayer AR, Mannell MV, Ling J, Gasparovic C, Yeo RA (2011) Functional connectivity in mild traumatic brain injury. *Hum Brain Mapp* 32(11):1825–1835
- Marino S, Ciurleo R, Bramanti P, Federico A, De Stefano N (2010) 1H-MR spectroscopy in traumatic brain injury. *Neurocrit Care* 14:127–133
- Gasparovic C, Yeo R, Mannell M, Ling J, Elgie R, Phillips J, Doezema D, Mayer A (2009) Neurometabolite concentrations in gray and white matter in mild traumatic brain injury: a 1H magnetic resonance spectroscopy study. *J Neurotrauma* 26(10):1635–1643
- Yeo RA, Gasparovic C, Merideth F, Ruhl D, Doezema D, Mayer AR (2011) A longitudinal proton magnetic resonance spectroscopy study of mild traumatic brain injury. *J Neurotrauma* 28:1–11
- Kirov II, George IC, Jayawickrama N, Babb JS, Perry NN, Gonen O (2012) Longitudinal inter- and intra-individual human brain metabolic quantification over 3 years with proton MR spectroscopy at 3 T. *Magn Reson Med* 67:27–33
- Tal A, Kirov II, Grossman RI, Gonen O (2012) The role of gray and white matter segmentation in quantitative proton MR spectroscopic imaging. *NMR Biomed*. doi:10.1002/nbm.2812
- Kreis R, Slotboom J, Hofmann L, Boesch C (2005) Integrated data acquisition and processing to determine metabolite contents, relaxation times, and macromolecule baseline in single examinations of individual subjects. *Magn Reson Med* 54:761–768
- Hu J, Javaid T, Arias-Mendoza F, Liu Z, McNamara R, Brown TR (1995) A fast, reliable, automatic shimming procedure using 1H chemical-shift-imaging spectroscopy. *J Magn Reson B* 108:213–219
- Goelman G, Liu S, Hess D, Gonen O (2006) Optimizing the efficiency of high-field multivoxel spectroscopic imaging by multiplexing in space and time. *Magn Reson Med* 56:34–40

23. Ashburner J, Friston K (1997) Multimodal image coregistration and partitioning – a unified framework. *Neuroimage* 6:209–217
24. Soher BJ, Young K, Govindaraju V, Maudsley AA (1998) Automated spectral analysis III: application to in vivo proton MR spectroscopy and spectroscopic imaging. *Magn Reson Med* 40:822–831
25. Traber F, Block W, Lamerichs R, Gieseke J, Schild HH (2004) ¹H metabolite relaxation times at 3.0 tesla: measurements of T1 and T2 values in normal brain and determination of regional differences in transverse relaxation. *J Magn Reson Imaging* 19:537–545
26. Kirov II, Fleysher L, Fleysher R, Patil V, Liu S, Gonen O (2008) Age dependence of regional proton metabolites T2 relaxation times in the human brain at 3 T. *Magn Reson Med* 60:790–795
27. Posse S, Otazo R, Caprihan A, Bustillo J, Chen H, Henry PG, Marjanska M, Gasparovic C, Zuo C, Magnotta V, Mueller B, Mullins P, Renshaw P, Ugurbil K, Lim KO, Alger JR (2007) Proton echo-planar spectroscopic imaging of J-coupled resonances in human brain at 3 and 4 Tesla. *Magn Reson Med* 58(2):236–244
28. Cecil KM, Hills EC, Sandel ME, Smith DH, McIntosh TK, Mannon LJ, Sinson GP, Bagley LJ, Grossman RI, Lenkinski RE (1998) Proton magnetic resonance spectroscopy for detection of axonal injury in the splenium of the corpus callosum of brain-injured patients. *J Neurosurg* 88:795–801
29. Govindaraju V, Gauger GE, Manley GT, Ebel A, Meeker M, Maudsley AA (2004) Volumetric proton spectroscopic imaging of mild traumatic brain injury. *AJNR Am J Neuroradiol* 25:730–737
30. Govind V, Gold S, Kaliannan K, Saigal G, Falcone S, Arheart KL, Harris L, Jagid J, Maudsley AA (2010) Whole-brain proton MR spectroscopic imaging of mild-to-moderate traumatic brain injury and correlation with neuropsychological deficits. *J Neurotrauma* 27:483–496
31. Garnett MR, Blamire AM, Rajagopalan B, Styles P, Cadoux-Hudson TA (2000) Evidence for cellular damage in normal-appearing white matter correlates with injury severity in patients following traumatic brain injury: a magnetic resonance spectroscopy study. *Brain* 123:1403–1409
32. Vagnozzi R, Signoretti S, Tavazzi B, Floris R, Ludovici A, Marziali S, Tarascio G, Amorini AM, Di Pietro V, Delfini R, Lazzarino G (2008) Temporal window of metabolic brain vulnerability to concussion: a pilot ¹H-magnetic resonance spectroscopic study in concussed athletes – part III. *Neurosurgery* 62:1286–1295 (discussion 1295–1296)
33. Vagnozzi R, Signoretti S, Cristofori L, Alessandrini F, Floris R, Isgro E, Ria A, Marziale S, Zoccatelli G, Tavazzi B, Del Bolgia F, Sorge R, Broglio SP, McIntosh TK, Lazzarino G (2010) Assessment of metabolic brain damage and recovery following mild traumatic brain injury: a multicentre, proton magnetic resonance spectroscopic study in concussed patients. *Brain* 133:3232–3242
34. Son BC, Park CK, Choi BG, Kim EN, Choe BY, Lee KS, Kim MC, Kang JK (2000) Metabolic changes in pericontusional oedematous areas in mild head injury evaluated by ¹H MRS. *Acta Neurochir* 76:13–16
35. Nakabayashi M, Suzuki S, Tomita H (2007) Neural injury and recovery near cortical contusions: a clinical magnetic resonance spectroscopy study. *J Neurosurg* 106:370–377
36. Kirov I, Fleysher L, Babb JS, Silver JM, Grossman RI, Gonen O (2007) Characterizing ‘mild’ in traumatic brain injury with proton MR spectroscopy in the thalamus: initial findings. *Brain Inj* 21:1147–1154
37. Farkas O, Povlishock JT (2007) Cellular and subcellular change evoked by diffuse traumatic brain injury: a complex web of change extending far beyond focal damage. *Prog Brain Res* 161:43–59
38. Graham DI, McIntosh TK, Maxwell WL, Nicoll JA (2000) Recent advances in neurotrauma. *J Neuropathol Exp Neurol* 59:641–651
39. Biasca N, Maxwell WL (2007) Minor traumatic brain injury in sports: a review in order to prevent neurological sequelae. *Prog Brain Res* 161:263–291
40. Kraus MF, Susmaras T, Caughlin BP, Walker CJ, Sweeney JA, Little DM (2007) White matter integrity and cognition in chronic traumatic brain injury: a diffusion tensor imaging study. *Brain* 130:2508–2519
41. Frahm J, Hanefeld F (1997) Localized proton magnetic spectroscopy of brain disorders in childhood. In: Bachelard HS (ed) *Magnetic resonance spectroscopy and imaging in neurochemistry*. Plenum Press, New York, pp 329–402
42. Di Giovanni S, Movsesyan V, Ahmed F, Cernak I, Schinelli S, Stoica B, Faden AI (2005) Cell cycle inhibition provides neuroprotection and reduces glial proliferation and scar formation after traumatic brain injury. *Proc Natl Acad Sci U S A* 102:8333–8338
43. Friedman SD, Brooks WM, Jung RE, Chiulli SJ, Sloan JH, Montoya BT, Hart BL, Yeo RA (1999) Quantitative proton MRS predicts outcome after traumatic brain injury. *Neurology* 52:1384–1391
44. Stein SC, Ross SE (1992) Mild head injury: a plea for routine early CT scanning. *J Trauma* 33:11–13
45. Borg J, Holm L, Cassidy JD, Peloso PM, Carroll LJ, von Holst H, Ericson K (2004) Diagnostic procedures in mild traumatic brain injury: results of the WHO collaborating centre task force on mild traumatic brain injury. *J Rehabil Med* (43 Suppl):61–75
46. Culotta VP, Sementilli ME, Gerold K, Watts CC (1996) Clinicopathological heterogeneity in the classification of mild head injury. *Neurosurgery* 38:245–250
47. Johnson VE, Stewart W, Smith DH (2012) Axonal pathology in traumatic brain injury. *Exp Neurol* (in press)
48. Baker EH, Basso G, Barker PB, Smith MA, Bonekamp D, Horska A (2008) Regional apparent metabolite concentrations in young adult brain measured by (¹H) MR spectroscopy at 3 Tesla. *J Magn Reson Imaging* 27:489–499
49. Ge Y, Grossman RI, Babb JS, Rabin ML, Mannon LJ, Kolson DL (2002) Age-related total gray matter and white matter changes in normal adult brain. Part I: volumetric MR imaging analysis. *AJNR Am J Neuroradiol* 23:1327–1333